Supplemental material for "Observation of infinite-range intensity correlations above, at, and below the mobility edges of the 3D Anderson localization transition"

W.K. Hildebrand,[1] A. Strybulevych,[1] S.E. Skipetrov,[2] B.A. van Tiggelen,[2] and J.H. Page[1]

[1] *Department of Physics and Astronomy, University of Manitoba, Winnipeg, Canada*
[2] *Université Grenoble 1/CNRS, LPMMC UMR 5493, B.P. 166, 38042 Grenoble, France*

(Dated: November 22, 2013)

This document provides a detailed description of how the experiments were performed and a summary of the theoretical results that were used to fit the data in the main text of the paper. Both the experimental procedure that was followed to conduct the ultrasonic measurements and the type of samples that were used are described. For the theory, we compute the short-, long- and infinite-range correlation functions of intensity under assumption of weak disorder $k\ell \gg 1$, where k is the wave number and ℓ is the mean free path due to disorder.

EXPERIMENTAL DETAILS

Samples

The samples investigated are disordered networks of aluminum beads, weakly brazed together to form disc-shaped slabs (see Fig. S1). The beads used are monodisperse and 4.11 ± 0.03 mm in diameter, and the samples have a volume fraction of approximately 55%, consistent with random loose packing. The beads were weakly bonded together by precisely controlling the flux, alloy concentration, and temperature during brazing, such that the spherical bead structure of the individual beads remained intact, with only small necks elastically connecting the beads. The samples were thoroughly cleaned to remove any surface contaminants from the beads that could lead to spurious dissipation in the ultrasonic experiments. The front and back surfaces of the samples were lightly polished to ensure that the opposite faces of the slabs were flat and parallel. The slabs were 120 mm in diameter, much larger than the sample thicknesses, in order that the slabs be sufficiently wide to avoid edge effects. Anderson localization has been observed in these samples for thicknesses L ranging from 8.3 to 23.5 mm [S1]. While correlation measurements were also performed for several sample thicknesses, the results shown in this paper are all for $L = 14.5$ mm, which was a representative data set for which the most complete results were obtained.

These samples exhibit very strongly scattering of ultrasound in the frequency range of the experiments, as we have determined by measuring the weak coherent signal that propagates ballistically through the sample [S1, S2]. Representative results of these measurements are shown in Table S1. At all frequencies, the scattering mean free path ℓ_s is considerably smaller than both the diameter of a single bead and the measured wavelength λ inside the samples, with the product of wave vector and mean free path $k\ell_s$ being of order unity.

FIG. S1. Photograph of one of the samples. Note the small "necks" connecting the beads, whose spherical shape is preserved. The lightly polished top surface is also visible.

TABLE S1. Experimentally determined parameters. The phase velocity, scattering mean free path, wavelength, and scattering strength are determined from ballistic measurements. The focal spot size was measured by scanning the hydrophone detector in the source plane.

Frequency	0.6 MHz	1.0 MHz	1.4 MHz	2.4 MHz
Ballistically measured parameters				
ℓ_s (mm)	1.0	0.7	0.8	0.6
v_p (mm/μs)	2.7	2.8	2.8	5.0
λ (mm)	4.5	2.8	2.0	2.1
$k\ell_s$	1.4	1.7	2.5	1.8
Focal spot size				
FWHM (mm)	1.5	1.2	0.93	0.91

Measurement procedures

The experiments were performed in a water tank to capitalize on the flexibility of ultrasonic immersion transducer technology for controlling source and detector po-

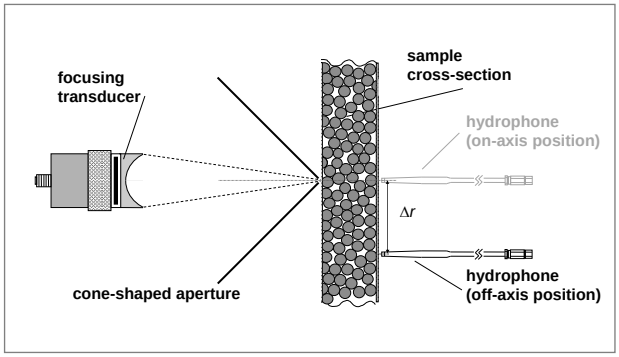

FIG. S2. Schematic diagram showing experimental setup.

sitions. A focused ultrasonic pulse was incident on the sample, and the transmitted waves were measured in the near field on the opposite side using a miniature hydrophone detector. A schematic representation of the experimental configuration is shown in Fig. S2.

Because we are interested in measuring ultrasonic transport through the solid elastic network of aluminum beads, the samples were mounted into acrylic holders and sealed with thin plastic walls to prevent water from entering the pore space surrounding the beads; hence, within the pores, only air (for the measurements at 2.4 MHz) or vacuum (for the lower frequency measurements between 0.5 and 1.5 MHz) was present. To ensure good acoustic coupling between the front and back sample surfaces and the flat waterproofing walls, the walls were coated with a very thin layer of an ultrasonic couplant.

The ultrasonic pulse was generated by focusing immersion transducers, which have front surfaces that are curved to act as a lens. The central frequencies of the transducers were either 1.0 or 2.25 MHz. The transducers were designed to have a focal length of approximately 30 cm, and a conical screen with a small aperture was placed at the focus to remove any side lobes or other beam artifacts. This large focal distance was selected to enable the multiply scattered, transmitted signals to be recorded before the arrival of any spurious echoes that had reverberated back and forth between the transducer and sample. Note also that this large focal distance ensured that the source was temporally decoupled from the sample, since the time interval between the emission of the pulse at the transducer and its arrival at the sample surface is very much longer than the incident pulse width. Thus, the pulse incident on the sample surface was a constant amplitude pressure pulse, with magnitude and bandwidth that was independent of the LDOS at the focal spot. This type of source has the advantage of simplicity for investigating the effect of LDOS fluctuations at the input surface on the intensity correlations of the transmitted signals, although its nature is quite different to sources in optics that have been used to investigate LDOS fluctuations themselves via the strong coupling that exists in the photonic environment around the sources and scatterers [S3]. In our experiments, for each source/detector location, the pulse was repeated several thousand times at a repetition rate of several hundred Hertz (slow enough to ensure that all signals due to the previous pulse had died completely away), so that the recorded signals could be averaged to improve the signal-to-noise ratio.

The conical screen was wrapped in Teflon tape to make it acoustically opaque. The cone shape was chosen so that edges of the focused beam could be effectively blocked when the aperture was placed close to the sample, while at the same time preventing significant stray sound being reflected back towards the sample from the screen. The pressure field at the source plane (about 1 mm from the aperture) was mapped using the hydrophone detector, so that the spatial extent of the source spot on the sample surface could be determined. The recorded signals were Fourier transformed and the intensity maps at each frequency were fit to a Gaussian in order to determine the source size. The results of these measurements are shown in Table S1. Note that the focal spot size at each frequency is significantly less than the wavelength inside the sample, and comparable to one wavelength in water.

The hydrophone used in these experiments is a subwavelength phase-sensitive detector with an active element diameter of 400 μm. The hydrophone has a needle-like shape, which serves to minimize reflections back to the sample. In our experiments, the hydrophone was placed approximately 1 mm from the sample surface (less than one wavelength in water), and thereby records the near-field transmission with good spatial resolution.

The intensity correlations of the transmitted ultrasonic waves were determined by first taking the Fourier transform of the recorded pressure fields $p(\mathbf{r}, t)$ and squaring the magnitude of the Fourier transforms to obtain signals that are proportional to the ultrasonic intensity at each frequency. Two types of experiments were performed in order to isolate the contributions to the intensity correlations of fluctuations in the local density of states at the source positions. The first set of experiments was designed to directly measure the C_0 correlations due to these LDOS fluctuations at the source. In these experiments, the transmitted signals were recorded at 13 detector positions for each source location. In order to get good statistics, the sample was scanned to have the source focused on over 3000 independent locations. For each pair of detector positions, the correlations were calculated for all source locations, and the results of the correlations for similar values of Δr were binned and averaged together. In the second set of experiments, which were designed to suppress these C_0 correlations, over 3000 detector positions were used for a single source location. Correlations were calculated for every possible

pair of detector positions, and results for similar values of Δr were again binned. This experiment was repeated for seven independent source locations, and the results of each of these experiments were averaged together.

THEORY FOR SPATIAL CORRELATIONS

Definitions

We consider the spatial correlation function of intensity fluctuations $\delta I(\mathbf{r},\omega) = I(\mathbf{r},\omega) - \langle I(\mathbf{r},\omega)\rangle$:

$$C_\omega(\mathbf{r},\mathbf{r}') = \frac{\langle \delta I(\mathbf{r},\omega)\delta I(\mathbf{r}',\omega)\rangle}{\langle I(\mathbf{r},\omega)\rangle\langle I(\mathbf{r}',\omega)\rangle}. \quad \text{(S1)}$$

To lighten the notation, we will omit the subscript 'ω' from here on, keeping in mind that all measurements are performed for waves at the same frequency ω. Typically, $C(\mathbf{r},\mathbf{r}')$ is a decaying function of $\Delta r = |\mathbf{r}-\mathbf{r}'|$ with $C(\mathbf{r},\mathbf{r}'=\mathbf{r}) = \langle \delta I(\mathbf{r})^2\rangle/\langle I(\mathbf{r})\rangle^2$ being the normalized variance of intensity, and $C(\mathbf{r},\mathbf{r}') = 0$ in the absence of intensity correlations. It is convenient to split $C(\mathbf{r},\mathbf{r}')$ in several parts: $C = C_1 + C_2 + C_3 + C_0$, each of C_i originating from different physical processes [S4, S5].

Short-range correlation C_1

In the bulk of a disordered medium and far from boundaries, the short-range contribution to C is [S4, S6]

$$C_1^{\text{bulk}}(\mathbf{r},\mathbf{r}') = \left(\frac{\sin k\Delta r}{k\Delta r}\right)^2 \exp(-\Delta r/\ell), \quad \text{(S2)}$$

where $k = 2\pi/\lambda$, ℓ is the scattering mean free path. At the surface of a disordered sample, the spatial correlation C_1 is modified due to the anisotropic angular distribution of intensity [S7]:

$$C_1^{\text{surface}}(\mathbf{r},\mathbf{r}') = \left\{\frac{1}{\Delta+\frac{1}{2}}\left[\Delta\frac{\sin k\Delta r}{k\Delta r} + \frac{J_1(k\Delta r)}{k\Delta r}\right]\right\}^2 \times \exp(-\Delta r/\ell) = h(k\Delta r, k\ell), \quad \text{(S3)}$$

where $\Delta = z_0/\ell^*$ with z_0 the extrapolation length entering the boundary conditions for the average intensity, and we defined the function $h(k\Delta r, k\ell)$ that will be used in the following. This result is largely independent of the spatial extent of the source (plane wave, beam of finite size or point source) and has been tested experimentally [S8].

The C_1 intensity correlation is equal to the square of the field correlation function, which we can measure directly since our detector records the transmitted pressure field. Our least-squares fits of the square root of Eq. (S3) to our experimental field correlation data yield values of the parameters k and ℓ that are consistent with those obtained from ballistic measurements [S2]. This indicates that Eq. (S3), with k and ℓ taken from ballistic measurements, gives a good description of our experimental results, which were obtained from measurements performed just outside the sample, within one wavelength of its surface. Thus, Eq. (S3) gives a reliable characterization of our experimental data for the C_1 contribution to the intensity correlation, supporting our use of this expression in our analysis of the total correlation $C_\omega(\mathbf{r},\mathbf{r}')$.

A more comprehensive study of the C_1 correlation would involve taking into account near-field effects in a way similar to a recent analysis published for electromagnetic waves [S9]. In any case, the precise form of C_1 does not play an important role in our analysis, which is mainly focused on the long-range correlations that are described next. We thus postpone a detailed analysis of C_1 to a future publication.

Long-range correlation C_2

In contrast to C_1, the long-range contribution C_2 depends on the spatial extent of the source. It is not easy to calculate for an arbitrary source. In addition, we have to make an assumption of weak disorder ($k\ell \gg 1$) to compute the diagrams corresponding to C_2.

Transmission of a plane wave through a slab. We assume that a slab of thickness $L \gg \ell$ and transverse extent $W \gg L$ is illuminated by a plane wave. The spatial correlation of intensity is calculated at the opposite side of the slab, as a function of transverse distance $\Delta r = |\mathbf{r}-\mathbf{r}'| \gg \ell^*$ [S10, S11]:

$$C_2^{\text{plane wave}}(\Delta r) = \frac{3}{2(k\ell^*)^2}\frac{\ell^*}{L}\left[\frac{L}{\Delta r} + F\left(\frac{\Delta r}{L}\right)\right] \simeq \begin{cases} \frac{3}{2(k\ell^*)^2}\frac{\ell^*}{\Delta r}, & \Delta r \ll L, \\ \propto e^{-\pi\Delta r/L}, & \Delta r > L, \end{cases} \quad \text{(S4)}$$

where

$$F(x) = \frac{1}{2}\int_0^\infty dq J_0(qx)\left(\frac{\sinh 2q - 2q}{\sinh^2 q} - 2\right), \quad \text{(S5)}$$

and ℓ^* is the transport mean free path.

Equation (S4) applies for $\Delta r \gg \ell^*$, where it exhibits the interesting slow decay, which is why this correlation function is often referred to as "long-range". However, the physical processes giving rise to this behavior are at work for $\Delta r \lesssim \ell^*$ as well. For $\Delta r = 0$, for example, they contribute to the variance of the intensity fluctuations $\langle \delta I(\mathbf{r})^2\rangle/\langle I(\mathbf{r})\rangle^2$. Physically, we expect $C_2(\Delta r = 0) \simeq C_2(\Delta r = \ell^*)$, but Eq. (S4) diverges for $\Delta r \to 0$. This divergence is an artifact of approximations made during the derivation of Eq. (S4). A more precise shape of $C_2(\Delta r)$ at small $\Delta r \lesssim \ell^*$ can be obtained by paying more attention to large q and avoiding the limit $q\ell^* \ll 1$ which is tacitly taken in the derivation

of Eq. (S4). We then obtain a longer but more accurate expression for C_2:

$$C_2^{\text{plane wave}}(\Delta r) = \frac{3}{2(k\ell^*)^2} F_2\left(\frac{\Delta r}{L}, \frac{\ell^*}{L}\right), \qquad \text{(S6)}$$

where

$$\begin{aligned} F_2(x,y) = \frac{y}{2}\int_0^\infty du \frac{J_0(ux)}{(uy\sinh u)^2} \big\{ &\sinh^2(uy) \\ &\times \left[\sinh[2u(1-y)] - 2u(1-y)\right] \\ &+ \sinh^2[u(1-y)]\left[\sinh(2uy) - 2uy\right]\big\} \\ \simeq &\begin{cases} 1-y, & x=0, \\ y/x, & y \ll x \ll 1, \\ \propto e^{-\pi x}, & x > 1. \end{cases} \end{aligned} \qquad \text{(S7)}$$

A comparison of Eqs. (S4) and (S6) is shown in Fig. S3. The latter equation, in contrast to Eq. (S4), allows us to obtain the value of C_2 for $\Delta r = 0$:

$$C_2^{\text{plane wave}}(\Delta r = 0) = \frac{3}{2(k\ell^*)^2}\left(1 - \frac{\ell^*}{L}\right). \qquad \text{(S8)}$$

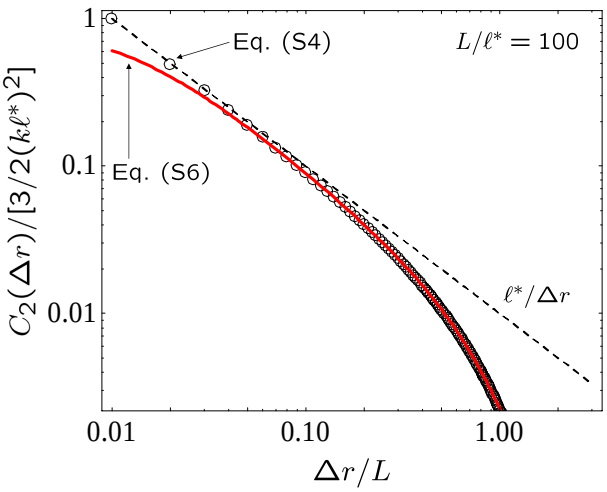

FIG. S3. Comparison of Eqs. (S4) (shown by circles) and (S6) (shown by the solid red line) for the long-range correlation function of intensity fluctuations. The dashed line shows $\ell^*/\Delta r$.

Point source in the infinite medium. Even if this geometry seems simple, the calculation of C_2 appears quite involved. If we define the center of mass $\mathbf{R} = \frac{1}{2}(\mathbf{r}_1 + \mathbf{r}_2)$ and the difference $\Delta\mathbf{r} = \mathbf{r}_1 - \mathbf{r}_2$ coordinates, we can obtain simple results for $\Delta\mathbf{r} \perp \mathbf{R}$:

$$C_2^{\text{point source}}(\Delta r) \simeq \pm\frac{3}{2(k\ell^*)^2}\frac{\ell^*}{\Delta r}, \qquad \text{(S9)}$$

with the '+' sign for $\Delta r \ll R$ and the '−' sign for $\Delta r \gg R$.

Transmission of a tightly focused beam through a slab. This situation is realized in our experiments and is somewhat intermediate with respect to the two previous cases (the sample is a slab, but the source is point-like). Because the results for the plane wave incident on a slab (S6) and the point source in the infinite medium (S9) coincide for $\ell^* < \Delta r < L$, we expect that the same result will also hold for the tightly focused beam. We will therefore use:

$$C_2^{\text{focused beam}}(\Delta r) \simeq \frac{3}{2(k\ell^*)^2} F_2\left(\frac{\Delta r}{L}, \frac{\ell^*}{L}\right), \quad \Delta r < L. \qquad \text{(S10)}$$

For $\Delta r > L$, we expect $C_2^{\text{focused beam}}(\Delta r)$ to be different from both Eqs. (S6) and (S9), but because its magnitude is already small at such large distances, it will not play a significant role in the fits to the experimental data.

Short-range part of C_2. The calculation leading to Eqs. (S6), (S9) and (S10) also yields short-range terms that are rarely mentioned but exist. The full expression for C_2 including both long- and short-range contributions is

$$C_2^{\text{full}}(\Delta r) \simeq \frac{3}{2(k\ell^*)^2}\left[F_2\left(0, \frac{\ell^*}{L}\right) h(k\Delta r, k\ell) + F_2\left(\frac{\Delta r}{L}, \frac{\ell^*}{L}\right)\right]. \qquad \text{(S11)}$$

Long-range correlation C_3

The calculation of the spatial C_3 correlation function for a beam focused on the surface of a 3D disordered slab is a complicated task that we did not succeed in accomplishing. However, the structure of the result may be anticipated from the diagrams involved in the calculation [S4]: we expect short- and long-range terms similar to C_2. The magnitude of C_3 is expected to be of order $1/(k\ell^*)^4$. Hence, an approximate expression for C_3 may be written as

$$C_3(\Delta r) \simeq \frac{\text{const}}{(k\ell^*)^4}\left[F_2\left(0, \frac{\ell^*}{L}\right) h(k\Delta r, k\ell) + F_2\left(\frac{\Delta r}{L}, \frac{\ell^*}{L}\right)\right]. \qquad \text{(S12)}$$

Infinite-range correlation C_0

Similarly to C_2 and C_3, C_0 correlation also contains the 'interesting', infinite-range part and the 'trivial', short-range one. The full expression is found by summing the

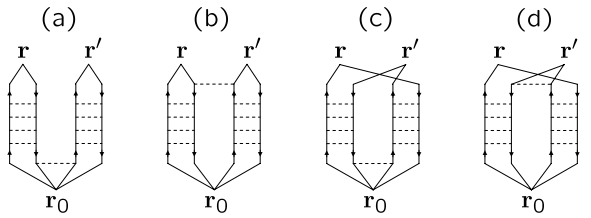

FIG. S4. Diagrams contributing to C_0 correlation function. $\mathbf{r}_0$ is the source position. The diagram (a) is the original long-range one [S5]; it is independent of $\Delta r = |\mathbf{r} - \mathbf{r}'|$. The diagram (b) is short-range. It was calculated in Ref. [S12]. The diagrams (c) and (d) are both short-range and were not considered previously. A complex conjugate diagram should be added to each of the diagrams.

diagrams of Fig. S4:

$$C_0^{(a)}(\Delta r) = C_0^{(\mathrm{in})}, \tag{S13}$$

$$C_0^{(b)}(\Delta r) = C_0^{(\mathrm{out})} \frac{f_b(k\Delta r, k\ell)}{f_b(0, k\ell)}, \tag{S14}$$

$$C_0^{(c)}(\Delta r) = C_0^{(\mathrm{in})} h(k\Delta r, k\ell), \tag{S15}$$

$$C_0^{(d)}(\Delta r) = C_0^{(\mathrm{out})} \frac{f_d(k\Delta r, k\ell)}{f_d(0, k\ell)}, \tag{S16}$$

where $C_0^{(\mathrm{in})}$ is the genuine, infinite-range correlation that survives at large Δr [S5]. It results from the scattering near the source and is related to the variance of the local density of states at $\mathbf{r}_0$ [S13]. In contrast, the terms (S14) and (S16), which are proportional to $C_0^{(\mathrm{out})}$, result from the scattering near the detection points $\mathbf{r}_1$ and $\mathbf{r}_2$. They are appreciable only at small $\Delta r = |\mathbf{r}_1 - \mathbf{r}_2|$. For the white-noise uncorrelated disorder, $C_0^{(\mathrm{in})} = C_0^{(\mathrm{out})} = \pi/k\ell$. In our experiment, the disorder is correlated and the symmetry between the 'point-like' excitation and the 'point-like' detection may be broken because neither is actually point-like and the effective sizes of the excitation and detection areas may differ, so that $C_0^{(\mathrm{in})} \neq C_0^{(\mathrm{out})} \neq \pi/k\ell$. Moreover, these parameters are not universal and will depend on the microscopic structure of the disordered sample [S14]. We use $C_0^{(\mathrm{in})}$ and $C_0^{(\mathrm{out})}$ as free fit parameters when comparing theory to the experimental data.

The functions $f_b(k\Delta r, k\ell)$ and $f_d(k\Delta r, k\ell)$ are rapidly

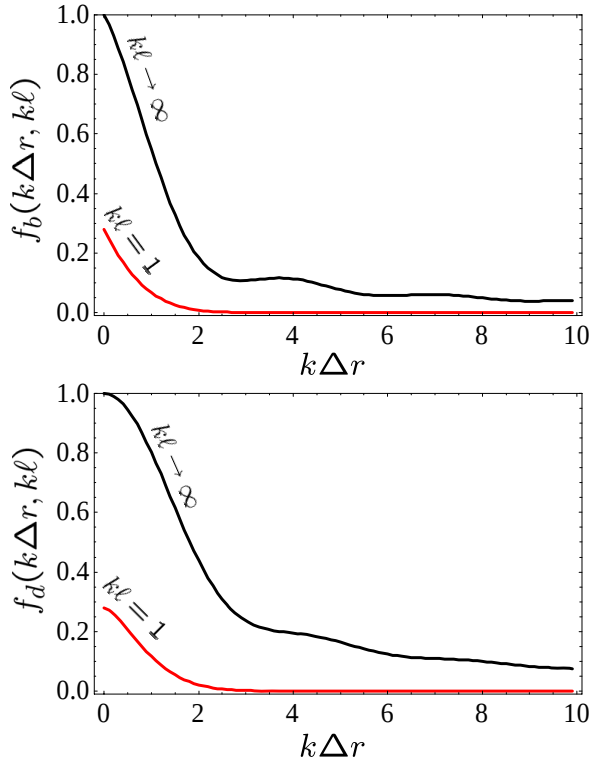

FIG. S5. Functions f_b and f_d describing the short-range part of C_0 correlation function.

decaying functions of $k\Delta r$:

$$\begin{aligned} f_b(k\Delta r, k\ell) = \frac{1}{2\pi k\Delta r} \mathrm{Re} \Big\{ i \int_0^\infty dx \frac{\sin x}{x} e^{-(i+1/k\ell)x} \\ \times \Big(\mathrm{Ei}[-(k\Delta r + x)/k\ell] \\ - \mathrm{Ei}[(2i - 1/k\ell)(k\Delta r + x)] \\ + \mathrm{Ei}[(2i - 1/k\ell)|k\Delta r - x|] \\ - \mathrm{Ei}[-|k\Delta r - x|/k\ell] \Big) \Big\}, \end{aligned} \tag{S17}$$

$$\begin{aligned} f_d(k\Delta r, k\ell) = \frac{1}{\pi k\Delta r} \int_0^\infty dx \frac{\sin^2 x}{x} e^{-x/k\ell} \\ \times \left[\mathrm{Ei}\left(-\frac{k\Delta r + x}{k\ell} \right) \right. \\ \left. - \mathrm{Ei}\left(-\frac{|k\Delta r - x|}{k\ell} \right) \right]. \end{aligned} \tag{S18}$$

The behavior of these functions is illustrated in Fig. S5.

Full expression for the correlation function

Adding up Eqs. (S3), (S11), (S12) and (S13)–(S16) we end up with an expression that can be used to fit

experimental data:

$$C(\Delta r) = \left[1 + A + C_0^{(\mathrm{in})}\right] h(k\Delta r, k\ell) + A \times \frac{F_2\left(\Delta r/L, \ell^*/L\right)}{F_2\left(0, \ell^*/L\right)} + C_0^{(\mathrm{in})} + C_0^{(\mathrm{out})} \left[\frac{f_b(k\Delta r, k\ell)}{f_b(0, k\ell)} + \frac{f_d(k\Delta r, k\ell)}{f_d(0, k\ell)}\right], \quad \text{(S19)}$$

where $A = [3/2(k\ell^*)^2 + \mathrm{const}/(k\ell^*)^4]F_2\left(0, \ell^*/L\right)$. A, $C_0^{(\mathrm{in})}$ and $C_0^{(\mathrm{out})}$ are the unknown fit parameters.

Role of the finite beam waist

In our experiments, the beam of ultrasound is focused to a small spot of size $w < \lambda$ on the sample surface, whereas theoretical results to which we compare our measurements are obtained for either an incident plane wave (C_1, C_2 and C_3) or a point source (C_1, C_2, C_3 and C_0). For the long-range correlations C_2 and C_3, this leads to the need of adjusting the parameter A to account empirically for the finite beam width when the comparison to experiments is made. Since A decreases as w increases [S11], our measurements underestimate the magnitude of the C_2 and C_3 correlations that would be measured for a true point-like source of waves. For the infinite-range C_0 correlation, having a source of finite size is known to reduce the magnitude of $C_0^{(\mathrm{in})}$ [S14], which is not exactly equal to the variance of LDOS anymore and will depend on w as well. Therefore, our measurements of C_0 underestimate the actual LDOS fluctuations, which are expected to be even stronger. However, the analysis presented in the main text of the paper does not rely on the magnitude of the correlations measured experimentally, but investigates their dependence on the distance between measurement points [Figs. 1 and 2(a)], the frequency difference [Fig. 2(b)], or the central frequency (Fig. 3). As a consequence, our conclusions remain valid independent of the beam waist w. A more detailed, quantitative comparison between theory and experiment would require calculating the dependence of C_2, C_3 and C_0 on w, so that the number of free parameters would be reduced in the fits presented in Figs. 1 and 2. However, such an analysis is beyond the scope of the present work and is not required to arrive at the conclusions that we make in the main text of the Letter.

Accounting for the size of the detector

In the experiment, the acoustic field is measured very close to the sample surface with a disk-shaped hydrophone of radius $b = 0.2$ mm. In order to take into account the size of the hydrophone, we assume that the measured quantity is not the intensity $I(\mathbf{r})$ at a point $\mathbf{r}$ but the intensity averaged over a disk of radius b centered at $\mathbf{r}$:

$$\mathcal{I}(\mathbf{r}) = \frac{1}{\pi b^2} \int_{b(\mathbf{r})} I(\mathbf{r}') d^2\mathbf{r}', \quad \text{(S20)}$$

where $b(\mathbf{r})$ denotes a disk of radius b centered at $\mathbf{r}$. The correlation function of $\mathcal{I}(\mathbf{r})$ can be then obtained from the correlation of $I(\mathbf{r})$ by a double spatial integration:

$$C_{\mathcal{I}}(\Delta\mathbf{r} = \mathbf{r}_1 - \mathbf{r}_2) = \frac{1}{(\pi b^2)^2} \int_{b(\mathbf{r}_1)} d^2\mathbf{r}_1' \int_{b(\mathbf{r}_2)} d^2\mathbf{r}_2' \times C_I(\Delta\mathbf{r}' = \mathbf{r}_1' - \mathbf{r}_2'). \quad \text{(S21)}$$

THEORY FOR FREQUENCY CORRELATIONS

Definitions

The frequency correlation function of intensity fluctuations $\delta I(\mathbf{r}, \omega) = I(\mathbf{r}, \omega) - \langle I(\mathbf{r}, \omega)\rangle$ is defined as

$$C_\omega(\mathbf{r}, \Omega) = \frac{\langle \delta I(\mathbf{r}, \omega + \frac{1}{2}\Omega)\, \delta I(\mathbf{r}, \omega - \frac{1}{2}\Omega)\rangle}{\langle I(\mathbf{r}, \omega)\rangle^2}, \quad \text{(S22)}$$

where we assume that the average intensity is independent of frequency in the frequency band under consideration: $\langle I(\mathbf{r}, \omega + \frac{1}{2}\Omega)\rangle = \langle I(\mathbf{r}, \omega - \frac{1}{2}\Omega)\rangle = \langle I(\mathbf{r}, \omega)\rangle$. Once again, we will omit the subscript 'ω' of C from here on. The behavior of $C(\mathbf{r}, \Omega)$ with Ω is similar to the behavior of the spatial correlation function $C(\Delta r)$ with Δr: it decays and has both short- and long-range parts.

Short-range correlation C_1

The short-range part of C can be easily calculated in transmission of a plane wave through a slab of thickness L [S4, S8]:

$$C_1(\Omega) = \left| \frac{L}{\ell^*} \times \frac{\sinh^2(\alpha\ell^*)}{\alpha\ell^* \sinh \alpha L} \right|^2, \quad \text{(S23)}$$

where $\alpha L = \pi\sqrt{i\Omega/\Omega_{\mathrm{Th}}}$, $\Omega_{\mathrm{Th}} = \pi^2 D/L^2$ is the Thouless frequency, D is the diffusion coefficient of the wave, and we neglected corrections due to boundary conditions, assuming $L \gg \ell^*, z_0$.

For a point source at the origin in the infinite medium we have

$$C_1(\mathbf{R}, \Omega) = \left|\exp\left(-\alpha R\right)\right|^2, \quad \text{(S24)}$$

with similar definitions $\alpha R = \pi\sqrt{i\Omega/\Omega_{\mathrm{Th}}}$, $\Omega_{\mathrm{Th}} = \pi^2 D/R^2$.

Both correlation functions (S23) and (S24) oscillate and decay roughly exponentially with $\sqrt{\Omega/\Omega_{\mathrm{Th}}}$, so that no correlation is left for $\Omega \gg \Omega_{\mathrm{Th}}$. We will adopt Eq. (S23) in the following.

Long-range correlation C_2

Transmission of a plane wave through a slab. From a calculation following Refs. [S11, S15] we found the following result:

$$C_2^{\text{plane wave}}(\Omega) = \frac{3}{2(k\ell^*)^2} F_2\left(\alpha L, \frac{\ell^*}{L}\right), \quad \text{(S25)}$$

where

$$F_2\left(\alpha L, \frac{\ell^*}{L}\right) = \frac{1}{2}\frac{L}{\ell^*}\int_0^\infty du\, u\, f\left(\frac{u}{L}, \alpha L, \frac{\ell^*}{L}\right), \quad \text{(S26)}$$

$$\begin{aligned} f\left(q, \alpha L, \frac{\ell^*}{L}\right) = \frac{4}{L}\Bigg[& \int_0^{\ell^*} dz \left(\frac{\sinh qz\ \sinh q\ell^*}{q\sinh qL}\right. \\ & \left.\times \left|\frac{\partial}{\partial z}\frac{\sinh \alpha z\ \sinh\alpha(L-\ell^*)}{\alpha\ell^*\ \sinh\alpha L}\right|\right)^2 \\ & + \int_{\ell^*}^{L-\ell^*} dz \left(\frac{\sinh qz\ \sinh q\ell^*}{q\sinh qL}\right. \\ & \left.\times \left|\frac{\partial}{\partial z}\frac{\sinh \alpha\ell^*\ \sinh\alpha(L-\ell^*)}{\alpha\ell^*\ \sinh\alpha L}\right|\right)^2 \\ & + \int_{L-\ell^*}^{L} dz \left(\frac{\sinh q(L-\ell^*)\ \sinh q(L-z)}{q\sinh qL}\right. \\ & \left.\times \left|\frac{\partial}{\partial z}\frac{\sinh \alpha\ell^*\ \sinh\alpha(L-\ell^*)}{\alpha\ell^*\ \sinh\alpha L}\right|\right)^2\Bigg]. \quad \text{(S27)} \end{aligned}$$

Integrations in this equation can be carried out analytically, resulting in a long expression that we do not reproduce here. Then the integral in Eq. (S26) can be calculated numerically.

In the limit of a thick slab $L \gg \ell^*$, Eq. (S25) yields a function that depends mainly on $\Omega/\Omega_{\text{Th}}$ as far as $\Omega/\Omega_{\text{Th}} \lesssim 1$, see Fig. S6 (top). In the limit of large $\Omega/\Omega_{\text{Th}} \to \infty$ we find

$$C_2^{\text{plane wave}}(\Omega) \propto C_2^{\text{plane wave}}(0) \times \frac{\ell^*}{L}\sqrt{\frac{\Omega_{\text{Th}}}{\Omega}}, \quad \text{(S28)}$$

as illustrated in Fig. S6 (bottom).

Point source in the infinite medium. Here we need to introduce a spatial cut-off $\sim \ell^*$ to avoid the path crossing (Hikami box) being closer than ℓ^* to the detector. The results then should be understood as depending on the precise value of this cutoff:

$$C_2^{\text{point source}}(\Omega) \simeq \frac{3}{4(k\ell^*)^2} F_2\left(\alpha R, \frac{\ell^*}{R}\right), \quad \text{(S29)}$$

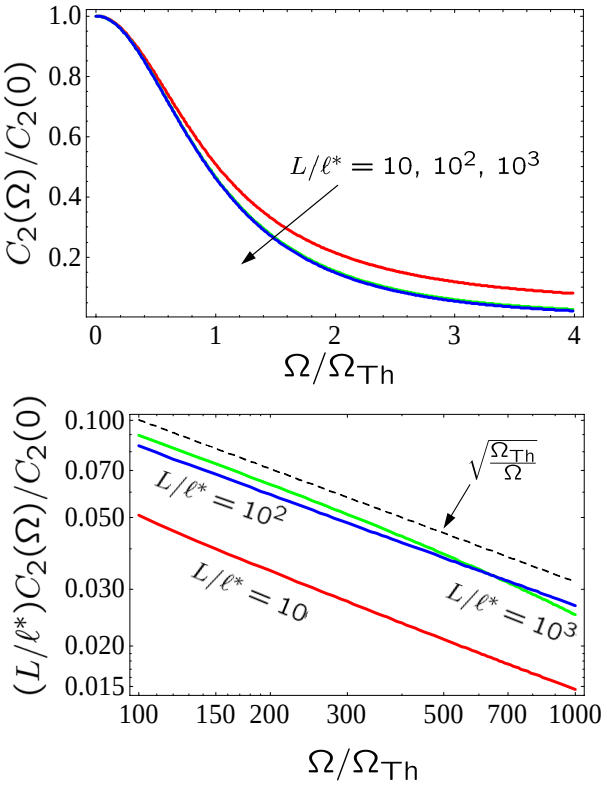

FIG. S6. Frequency correlation of intensity fluctuations C_2 in transmission of a plane wave through a disordered slab for small (top) and large (bottom) values of Ω.

where

$$F_2\left(\alpha R, \frac{\ell^*}{R}\right) = 2\frac{\ell^*}{R}\left\{\int_0^{1-\ell^*/R} dx \frac{\exp[-2\text{Re}(\alpha R)x]}{(1-x^2)^2} + \int_{1+\ell^*/R}^{\infty} dx \frac{\exp[-2\text{Re}(\alpha R)x]}{(1-x^2)^2}\right\}. \quad \text{(S30)}$$

In the limit of $R \gg \ell^*$ that is of interest for us here, we have

$$F_2\left(0, \frac{\ell^*}{R}\right) = 1, \quad \text{(S31)}$$

$$F_2\left(\alpha R, \frac{\ell^*}{R}\right) = \frac{\ell^*}{R} \times \frac{1}{\text{Re}(\alpha R)}, \quad \Omega \gg \Omega_{\text{Th}} \quad \text{(S32)}$$

The behavior of C_2 at small and large Ω is illustrated in Fig. S7.

Transmission of a tightly focused beam through a slab. We assume that the C_2 correlation function for a beam focused on the surface of a disordered slab is similar to the one for the plane wave, except for the magnitude

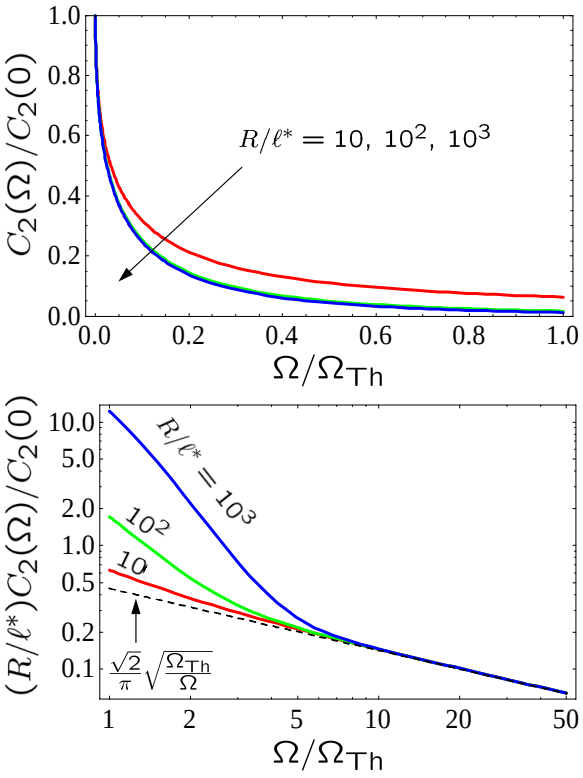

FIG. S7. Frequency correlation of intensity fluctuations C_2 at a distance R from a point source in the infinite medium for small (top) and large (bottom) values of Ω.

of C_2 [S15]:

$$C_2^{\text{focused beam}}(\Omega) \simeq \frac{\text{const}}{(k\ell^*)^2} F_2\left(\alpha L, \frac{\ell^*}{L}\right), \quad \text{(S33)}$$

with $F_2(\alpha L, \ell^*/L)$ defined by Eq. (S26).

Infinite-range correlation C_0

The frequency dependence of the C_0 correlation function is obtained by calculating the diagrams of Fig. S8. We obtain:

$$C_0^{(a)}(\Omega) = C_0^{(\text{in})}, \quad \text{(S34)}$$
$$C_0^{(b)}(\Omega) = C_0^{(\text{out})}, \quad \text{(S35)}$$
$$C_0^{(c)}(\Omega) = C_0^{(\text{in})} C_1(\Omega), \quad \text{(S36)}$$
$$C_0^{(d)}(\Omega) = C_0^{(\text{out})} C_1(\Omega). \quad \text{(S37)}$$

Full expression for the correlation function

Adding up all the contributions and assuming (as in the case of spatial correlations) that the behavior of C_3

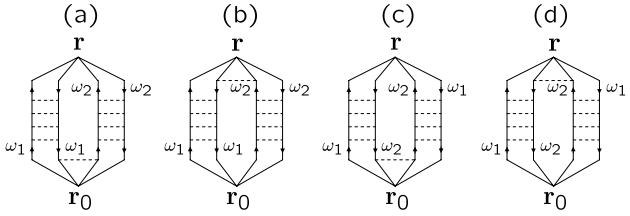

FIG. S8. Diagrams contributing to C_0 correlation function. $\mathbf{r}_0$ is the source position; $\omega_{1,2} = \omega \pm \frac{1}{2}\Omega$. The diagrams (a) and (b) are independent of $\Omega = \omega_1 - \omega_2$ as far as $|\Omega| \ll \omega_{1,2}$. A complex conjugate diagram should be added to each of the diagrams.

as a function of frequency is similar to that of C_2, we finally find the full expression for the frequency correlation function:

$$C(\Omega) = \left[1 + C_0^{(\text{in})} + C_0^{(\text{out})}\right] C_1(\Omega) + 2A \times \frac{F_2(\alpha L, \ell^*/L)}{F_2(0, \ell^*/L)} + C_0^{(\text{in})} + C_0^{(\text{out})}, \quad \text{(S38)}$$

where $A \sim 1/(k\ell^*)^2$. Note that the constants A and $C_0^{(\text{in,out})}$ here should be the same as in Eq. (S19) for the spatial correlation.

[S1] H. Hu, A. Strybulevych, J. H. Page, S. E. Skipetrov, and B. A. van Tiggelen, Nature Phys. **4**, 945 (2008).
[S2] J. H. Page, P. Sheng, H. P. Schriemer, I. P. Jones, X. Jing, and D. A. Weitz, Science **271**, 634 (1996).
[S3] R. G. S. El-Dardiry, S. Faez, and A. Lagendijk, Phys. Rev. A **83**, 031801 (2011).
[S4] E. Akkermans and G. Montambaux, *Mesoscopic Physics of Electrons and Photons* (Cambridge University Press, Cambridge, 2007).
[S5] B. Shapiro, Phys. Rev. Lett. **83**, 4733 (1999).
[S6] B. Shapiro, Phys. Rev. Lett. **57**, 2168 (1986).
[S7] I. Freund and D. Eliyahu, Phys. Rev. A **45**, 6133 (1992).
[S8] P. Sebbah, R. Pnini, and A. Z. Genack, Phys. Rev. E **62**, 7348 (2000).
[S9] R. Carminati, Phys. Rev. A **81**, 053804 (2010).
[S10] M. J. Stephen and G. Cwilich, Phys. Rev. Lett. **59**, 285 (1987).
[S11] R. Pnini and B. Shapiro, Phys. Rev. B **39**, 6986 (1989).
[S12] A. Retzker and B. Shapiro, Pramana **58**, 225 (2002).
[S13] B. A. van Tiggelen and S. E. Skipetrov, Phys. Rev. E **73**, 045601 (2006).
[S14] S. E. Skipetrov and R. Maynard, Phys. Rev. B **62**, 886 (2000).
[S15] J. F. de Boer, M. P. van Albada, and A. Lagendijk, Phys. Rev. B **45**, 658 (1992).